

1 **Size distribution and mixing state of black carbon particles during a heavy air
2 pollution episode in Shanghai**

3 Xianda Gong¹, Ci Zhang¹, Hong Chen¹, Sergey A. Nizkorodov², Jianmin Chen^{1,3}, Xin
4 Yang^{1,3*}

5 1 Shanghai Key Laboratory of Atmospheric Particle Pollution and Prevention,
6 Department of Environmental Science and Engineering, Fudan University, Shanghai
7 200433, China

8 2 Department of Chemistry, University of California, Irvine, California 92697, United
9 States

10 3 Fudan-Tyndall Center, Fudan University, Shanghai 200433, China

11 Correspondence to: Xin Yang (yangxin@fudan.edu.cn)

12 **Abstract:** A Single Particle Aerosol Mass Spectrometer (SPAMS), a Single Particle Soot
13 Photometer (SP2) and various meteorological instruments were employed to investigate
14 the chemical and physical properties of black carbon (BC) aerosols during a regional air
15 pollution episode in urban Shanghai over a five-day period in December 2013. The
16 refractory black carbon (rBC) mass concentrations measured by SP2 averaged $3.2 \mu\text{g m}^{-3}$,
17 with the peak value of $12.1 \mu\text{g m}^{-3}$ at 04:26 LT on 7 December. The number of
18 BC-containing particles captured by SPAMS in the size range 200-1200 nm agreed very
19 well with that detected by SP2 ($R^2 = 0.87$). A cluster analysis of the single particle mass
20 spectra allowed for the separation of BC-containing particles into five major classes: (1)
21 Pure BC; (2) BC attributed to biomass burning (BBC); (3) K-rich BC-containing (KBC);
22 (4) BC internally-mixed with OC and ammonium sulfate (BCOC-SOx); (5) BC
23 internally-mixed with OC and ammonium nitrate (BCOC-NOx). The size distribution of
24 internally-mixed BC particles was bimodal. Detected by SP2, the condensation mode
25 peaked around ~ 230 nm and droplet mode peaked around ~ 380 nm, with a clear valley in
26 the size distribution around ~ 320 nm. The condensation mode mainly consisted of traffic
27 emissions, with particles featuring a small rBC core (~ 60 -80 nm) and a relatively thin
28 absolute coating thickness (ACT, ~ 50 -130 nm). The droplet mode included highly aged
29 traffic emission particles and biomass burning particles. The highly aged traffic emissions

had a small core (~60-80 nm) and a very thick ACT (~130-300 nm), which is larger than reported in any previous literature. A fast growth rate (~20 nm h⁻¹) of rBC with small core sizes was observed during the experiment. The biomass burning particles had a larger rBC core (~80-130 nm) and a thick ACT (~110-300 nm). High concentrations pollutants like NO₂ likely accelerated the aging process and resulted in a continuous size growth of rBC-containing particles from traffic emission.

1 Introduction

Aerosols represent the largest uncertainty in estimating radiative forcing of atmospheric species, through strongly affecting the energy balance of the Earth by scattering and/or absorbing solar radiation (Pöschl, 2005), and influencing cloud formation (Jacobson, 2006). Emitted from incomplete combustion of fossil fuel and biomass (Bond et al., 2013), black carbon (BC) is a strongly light-absorbing carbonaceous material in aerosols, second to carbon dioxide as a contributor to positive radiative forcing (Ramanathan and Carmichael, 2008; Jacobson, 2001).

The physical (e.g., size distribution and morphology) and chemical (e.g., mixing state and composition) properties of ambient BC are very complex and are constantly changing in the atmosphere. For example, BC particles exposed to sub-saturated sulfuric acid vapor exhibit a marked change in morphology, characterized by a decreased mobility-based diameter but an increased fractal dimension and effective density (Zhang et al., 2008). Through using electron tomography with a transmission electron microscope and three-dimensional (3-D) imaging, Adachi et al. (2010) found that many BC particles have open, chainlike morphology even after being surrounded by organic matter, and are located in off-center positions within their host materials. China et al. (2013) analyzed the morphology of single BC particles using electron microscopy and classified them into four categories: ~50% were embedded (heavily coated), ~34% were partly coated, ~12% had inclusions and ~4% were bare. The organic coating is known to strongly affect the optical properties of the soot aggregates by acting as a lens that amplifies the absorption cross section of the BC core (Lack and Cappa, 2010; Shiraiwa et al., 2010). Schnaiter et al. (2005) observed that amplification factors of the internally-mixed BC of 1.8 to 2.1

relative to the specific absorption cross section of externally-mixed BC. Zhang et al. (2008) observed that the internally-mixed particles can increase their absorption efficiency by nearly 2-fold and scattering efficiency by approximately 10-fold at 80% relative humidity relative to fresh particles. On the other hand, Cappa et al. (2012) and Lan et al. (2013) observed a limited enhancement due to the mixing state of ambient BC, suggesting that other factors may affect their absorption properties. Through coagulation and condensation, BC can form an internal mixture, which increases its cloud nucleation activity (Khalizov et al., 2009; Moffet and Prather, 2009). Most BC is removed from the troposphere via wet deposition with a short lifetime of 5 to 10 days (Kanakidou et al., 2005; Chung and Seinfeld, 2002).

Many measurement methods for refractory BC (rBC) particles have been developed and used in recent years (Petzold et al., 2013). Among them, the Single Particle Soot Photometer (SP2) has become increasingly recognized as a valuable tool for characterizing rBC-containing particles (Stephens et al., 2003; Schwarz et al., 2006). SP2 can quantitatively measure the mass and determine the mixing state of an individual rBC-containing particle (Schwarz et al., 2010). Taylor et al. (2014) evaluated the capability of the SP2 to determine the particle mixing state through using the concentric core/shell model. Liu et al. (2014) analyzed the size distribution and mixing state of rBC aerosols in London during winter time based on the same technique. Furthermore, Moteki et al. (2014) identified two morphological types of the mixed rBC-containing particles as attached and coated, an important finding for understanding the climate impact of rBC particles. Recently, a soot particle aerosol mass spectrometer (SP-AMS) was developed to characterize rBC and non-refractory particulate matter simultaneously (Cross et al., 2010; Onasch et al., 2012; Corbin et al., 2014). SP-AMS was previously used to quantify rBC mass concentration, mixing state and chemical composition in urban environment and biomass burning influenced air (Lee et al., 2015a; Lee et al., 2015b; Willis et al., 2015).

As a highly complementary instrument, single particle aerosol mass spectrometer (SPAMS, not to be confused with the SP-AMS instrument mentioned above) can detect

88 the chemical properties of BC particles. Moffet and Prather (2009) observed a rapid
89 coating process of organic carbon and sulfate on the BC core and assessed the related
90 absorption enhancement during an air pollution episode of the Mexico City. Healy et al.
91 (2012b) found that the mass size distribution for BC-containing particles was bimodal at
92 an urban background site in Paris. The smaller mode was attributed to local emission,
93 mostly externally-mixed BC particles, while the larger mode was dominated by aged
94 particles associated with continental transport events. Zhang et al. (2014) found that an
95 active photochemical formation of secondary organic aerosol (SOA) led to a distinct
96 diurnal pattern of mixing state of BC with SOA in the condensation mode, while the
97 photochemical aging had limited or negligible influence on the mixing state and growth
98 of BC in the droplet mode. The size ranges of condensation mode (Vacuum Aerodynamic
99 Diameter (D_{va})= ~100-300 nm) and droplet mode (D_{va} = ~300- 1000 nm) were defined by
100 John et al. (1990) and Seinfeld and Pandis (2012).

101 Depending on the experimental method, different terms are used in the literature for the
102 most refractory and light-absorbing components of carbonaceous aerosols: black carbon
103 (BC), refractory black carbon (rBC) and elemental carbon (EC). The definitions of BC,
104 rBC and EC have been discussed in details elsewhere (Bond and Bergstrom,
105 2006;Almeida et al., 2013;Petzold et al., 2013). In this paper, we use rBC and BC to
106 illustrate the SP2 and SPAMS data, respectively.

107 All of the studies mentioned above relied on either an SP2 instrument or a single particle
108 mass spectrometer to characterize BC particles. Combining these two methods would
109 provide the chemical and physical prosperities of individual BC particles simultaneously
110 and greatly enhance our understanding of their sources and evolution processes.
111 Furthermore, most previous SP2 studies focused on the BC particles during relatively
112 clean days. Quantitative analysis on the mixing state of BC particles during heavy
113 pollution episodes is still lacking. In this study, we deployed two complementary
114 techniques, with single particle resolution and high time resolution, to detect the
115 evolution of the urban BC aerosols in Shanghai during an extreme pollution period. We
116 used an SP2 instrument to measure the mass and size distribution, and the mixing state of

117 individual rBC particles. A SPAMS instrument was used in parallel to record chemical
118 characteristics and mixing state of individual BC particles.

119 **2 Experimental**

120 **2.1 Single Particle Soot Photometer**

121 **2.1.1 Description**

122 The number and mass size distribution, as well as the mixing state of individual rBC
123 particles were characterized using a single particle soot photometer (SP2, Droplet
124 Measurement Technologies, Inc., Boulder, CO) (Stephens et al., 2003; Baumgardner et al.,
125 2004). In brief, SP2 detects incandescence and scattering signals of rBC-containing
126 particles induced by a 1064 nm Nd: YAG intra-cavity laser. The mass of rBC is
127 proportional to the intensity of the laser induced incandescence signal. Any measured
128 particle with a detectable incandescence signal is treated as an rBC particle; whereas a
129 particle that only exhibits scattering signal is considered as a non-rBC particle. The total
130 rBC mass loading is reported as the sum of all detected single rBC masses. The SP2
131 instrument samples at low flow ($30 \text{ cm}^3 \text{ min}^{-1}$) in order to avoid multiple particles
132 crossing the laser at the same time. We only saved data for every 50th particle in order to
133 extend the sampling time without generating excessively large data sets.

134 **2.1.2 Calibration and detection efficiency**

135 The SP2 incandescence signal was calibrated using Aquadag® black carbon particles
136 (Aqueous Deflocculated Acheson Graphite, manufactured by Acheson Inc., USA). The
137 Aquadag® black carbon particles were selected by mobility diameter using a differential
138 mobility analyzer (DMA) and the corresponding particle masses were calculated using
139 the effective density data provided in Gysel et al. (2011) (Fig. S1). The scattering signal
140 was calibrated using mono-disperse polystyrene latex spheres (Nanosphere Size
141 Standards, Duke Scientific Corp., Palo Alto, CA, USA) with known diameters (80–350
142 nm). More details about the SP2 calibration can be found in Gysel et al. (2011),

143 Baumgardner et al. (2012) and Laborde et al. (2012). A diagram of the calibration system
144 is shown in the supplement (Fig. S2).

145 The detection efficiency was measured using Aquadag® black carbon particles, and the
146 results are shown in Fig. S3. The details of the measurement method were described in
147 Schwarz et al. (2010). SP2 detection efficiency was nearly unity for larger rBC particles.
148 The minimum rBC mass that could be observed with near-unity detection efficiency was
149 ~ 0.7 fg rBC, corresponding to 90 nm mass-equivalent diameter; the detection efficiency
150 declined rapidly at lower sizes (Fig. S3). The total ambient mass concentrations of rBC
151 were underestimated because of the low detection efficiency of the smaller rBC particles,
152 likely by ~20 % (Schwarz et al., 2006; McMeeking et al., 2010). During the calibration
153 and sampling time, the SP2 was operated at a stable temperature 20 °C and pressure
154 ~1013 hPa. The SP2 laser current was at 1750 mA through the whole experiment.

155 **2.1.3 Data analysis**

156 The rBC mass in each individual particle was determined from the peak intensity of the
157 incandescence signal according to the Aquadag® black carbon calibration (Sect. 2.1.2).
158 The measured ambient rBC mass was converted to the mass equivalent diameter,
159 assuming a density of 1.8 g cm⁻³ (Bond and Bergstrom, 2006). In addition to the rBC
160 mass, the measurement of the scattering signal of a rBC-containing particle allows for the
161 determination of its scattering cross section. However, the scattering properties of
162 externally- and internally-mixed rBC particles, as detected by the SP2, may be distorted,
163 because the mass of each particle is reduced by the laser heating. Thus, scattered light
164 from a sampled rBC particle does not yield a full Gaussian waveform. The Gaussian
165 scattering function was reconstructed from the leading edge of the scattering signal
166 (before the particle is perturbed by the laser), which was measured with a two-element
167 avalanche photodiode (APD). This method allows SP2 to determine the scattering
168 properties of individual rBC particles as well as the rBC mass and to distinguish the
169 mixing state of a single rBC particle (so called, LEO-fit method (Gao et al., 2007)). The
170 optical diameter of a rBC particle or the coated rBC size (D_p) was derived by inputting
171 the LEO fitted scattering signal and rBC core size (D_c) into Mie calculations, and using a

core refractive index $m = 2.26 - 1.26i$ (Moteki et al., 2010; Liu et al., 2014; Laborde et al., 2013) and a coating refractive index $m = 1.5 + 0i$ (Laborde et al., 2013). The absolute coating thickness (ACT) of a rBC particle was calculated as $(D_p - D_c)/2$, based on the assumption of a concentric core-shell morphology. However, rBC aging processes in the real atmosphere may result in aerosols with particles that have a morphology that deviates from the core-shell model (Matsui et al., 2013). For example, when a small rBC particle coagulates with a relatively large rBC-free particle, the small rBC particle may stay at the surface and lead to an effective negative coating thickness if determined by the methods used here. In this study, the negative coating thickness was observed for less than 2% of all rBC-containing particles; we did not take those particles into account when we calculated the average ACT. More details of data analysis and uncertainties are discussed in supplement, as well as in Liu et al. (2014) and Laborde et al. (2013).

2.2 Single Particle Aerosol Mass Spectrometer

A SPAMS instrument (Hexin Analytical Instrument Co., Ltd., Guangdong, China) was deployed simultaneously with SP2 to detect chemical composition of BC-containing particles. The technical details of SPAMS have been described elsewhere (Li et al., 2011). Briefly, aerosols in the size range of 0.2–2.0 μm are introduced into the focus lens through a 0.1 mm critical orifice at a flow of 80 mL min^{-1} due to the pressure drop from ~760 to ~2.2 Torr. Then particles are accelerated to a terminal size-dependent aerodynamic velocity, which is measured by two orthogonally-oriented continuous lasers (532 nm) separated by a fixed 6.0 cm distance. A pulsed desorption/ionization laser (Q-switched Nd: YAG laser, 266 nm) is triggered when a particle arrives at the ion source region. Both positive and negative ions are detected simultaneously by the time-of-flight mass spectrometer. In this work, the power of the desorption/ionization laser was kept at ~0.6 mJ per pulse. The particle size was calculated from the measured speed using a calibration curve generated by mono-disperse polystyrene latex spheres (Nanosphere Size Standards, Duke Scientific Corp., Palo Alto, CA, USA) with known diameters (0.22–2.00 μm).

200 All single particle mass spectra were converted into a list of peaks at each m/z using TSI
201 MS-Analyze software with a minimum signal threshold of 30 arbitrary units above the
202 baseline. The resulting peak lists were then imported into YAADA (www.yaada.org), a
203 software toolkit in Matlab (version R2012b) for further analysis of particle sizes and
204 chemical components. A total of 385 683 particles were chemically analyzed with both
205 positive and negative ion spectra, accounting for about 56 % of all sized particles. Based
206 on the similarities of the mass-to-charge ratio and peak intensity, particles were clustered
207 by using the ART-2a (adaptive resonance theory) method (Song et al., 1999) with a
208 vigilance factor of 0.85, a learning rate of 0.05 and 20 iterations. Then BC-containing
209 particles, with D_{va} in the size range of 200-1200 nm, were chosen from the clusters, since
210 this size range was consistent with the dominant fraction of BC-containing mass in the
211 atmosphere (Zhang et al., 2014;Healy et al., 2012b). Finally, a total of 86 057
212 BC-containing particles were grouped into six general particle types according to mass
213 spectral patterns.

214 **2.3 Monitor for AeRosols and GAses (MARGA)**

215 A MARGA instrument (ADI 2080, Applikon Analytical B. B. Corp., Netherlands) was
216 used to measure water-soluble inorganic ions in particles. The details of MARGA have
217 been described previously (Jongejan et al., 1995;Du et al., 2011). Briefly, air to be
218 analyzed enters into sample boxes via a PM₁ cyclone. The air flow is maintained at 1 m³
219 h⁻¹ by a mass flow controlled air pump. In the sample box, water-soluble gases (HCl,
220 HONO, SO₂, HNO₃, NH₃) are completely absorbed in a dilute solution of hydrogen
221 peroxide by using a wet rotating denuder (WRD). Aerosols pass through the WRD and
222 are subsequently collected in a steam-jet aerosol collector (SJAC). The two liquid
223 samples with absorbed gases and particles are accumulated in syringes in the analytical
224 box. After filling the syringes for one hour, the samples are then injected into an ion
225 chromatograph (IC). The IC is continuously controlled by an internal calibration method
226 using a standard LiBr solution. In this study, the water-soluble inorganic ions (i.e., K⁺,
227 SO₄²⁻, NO₃⁻) in bulk particles were analyzed.

228 **2.4 Sampling period and site**

229 The sampling lasted for almost 5 days, from 5 to 10 December, 2013. The instruments
230 were operated in the building of the Department of Environmental Science and
231 Engineering, Fudan University (FDU, 31° 14' N, 121° 29' E) in urban Shanghai, close
232 to both residential and traffic emissions sources. Aerosols were sampled with a PM_{2.5}
233 cyclone positioned 2 m above the roof of the building and transferred to the instruments
234 through a 6 m long stainless steel pipe (45 mm inner diameter). A pump was used to pull
235 air through the sampling system at 30 L min⁻¹, minimizing the particle residence time in
236 the sampling line. Aerosols were dried by diffusion drying tubes before they reached the
237 SP2 and SPAMS inlets, which were connected in parallel. The measurement system is
238 presented in Fig. S2. Because of the extremely high particle mass loading, the inlets of
239 SP2 and SPAMS were clogged two times during the sampling period.

240 **3 Result and discussion**

241 **3.1 Overview of the meteorology and air quality**

242 Temporal variations of measured relative humidity, temperature, CO, O₃, NO, NO₂, SO₂,
243 PM_{2.5} and PM₁₀ in Shanghai from 12:00 LT on 5 December to 14:00 LT on 10 December
244 are shown in Fig. 1. The meteorology and air quality information were provided by the
245 Shanghai Environmental Monitoring Center, Hongkou Station
246 (<http://www.semc.com.cn/aqi/home/Index.aspx>). The station is 3.3 km north from the
247 sampling site. The temperature and relative humidity varied between 2-19 °C and
248 30-100%, with an average of 19 °C and 73%, respectively, during the study. The O₃
249 concentration was relatively low from 18:00 LT on 5 December to 8:00 LT on 7
250 December. The CO concentration showed two peaks during this period, and its peak
251 value reached 4.1 mg m⁻³ at 14:00 LT on 6 December. The NO₂ concentration increased
252 quickly at the beginning, reached 202.5 µg m⁻³ at 21:00 LT on 5 December, and then
253 decreased slowly until 12:00 LT on 7 December. After 12:00 LT on 7 December, the
254 concentrations of O₃, CO, NO₂ and SO₂ fluctuated without an obvious pattern. The
255 concentrations of O₃ and NO₂ showed the expected anti-correlation, because NO was
256 oxidized to NO₂ by O₃. The CO concentration was found to correlate reasonably well
257 with rBC mass concentration ($R^2=0.59$, slope=0.33), as shown in Fig. S4.

258 The mass loading of PM_{2.5} was extremely high during this period. Its maximum value
259 reached 636 $\mu\text{g m}^{-3}$ at 12:00 LT on 6 December, which was a record-breaking hourly
260 concentration for Shanghai. The daily average concentration was 221 $\mu\text{g m}^{-3}$. Meanwhile,
261 PM₁₀ varied from 47 to 691 $\mu\text{g m}^{-3}$, with an average of 252 $\mu\text{g m}^{-3}$. Concentrations of CO,
262 O₃, NO, NO₂, SO₂, PM₁₀ and PM_{2.5} during 5-10 December all exceeded the Chinese
263 national ambient air quality standards.

264 **3.2 BC size distributions and concentration measurement by SP2**

265 We fitted a log-normal distribution to the rBC core number and mass size measurements
266 during the entire sampling period, as shown in Fig. 2. The number size ranged from ~60
267 to ~400 nm and the peak was around ~60 nm. The measured number concentrations
268 dropped below 60 nm because the SP2 detection efficiency greatly decreases (Sect. 2.1.2)
269 below this particle size. Using the same method, Schwarz et al. (2008) also found that the
270 peak concentration was around 60 nm in boundary layer. The rBC core mass size
271 distribution had a peak around 200 nm, and the most rBC mass was distributed between
272 70-500 nm.

273 As shown in Fig. 1, the rBC mass concentration varied from 0.6 $\mu\text{g m}^{-3}$ at 00:02 LT on
274 10 December to 12.1 $\mu\text{g m}^{-3}$ at 04:26 LT on 7 December, with an average of 3.2 $\mu\text{g m}^{-3}$.
275 The rBC mass concentration observed in Shanghai was similar to other cities in China,
276 e.g., ~4.1 $\mu\text{g m}^{-3}$ in Shenzhen (Huang et al., 2012) and ~3.3 $\mu\text{g m}^{-3}$ in Kaiping (Huang et
277 al., 2011). However, it was much higher than in other mega-cities around the world, e.g.,
278 ~0.9 $\mu\text{g m}^{-3}$ in Paris (Laborde et al., 2013) and ~1.3 $\mu\text{g m}^{-3}$ in London (Liu et al., 2014).
279 All of the values quoted above were based on SP2 measurement. The rBC mass
280 accounted for 1.45% of PM_{2.5} mass on average in our measurements.

281 **3.3 BC particles classification by SPAMS**

282 Classification of particles analyzed by the SPAMS can help elucidate the sources, degree
283 of aging, and mixing state of BC particles. We classified BC-containing particles into six
284 groups according to their mass spectral characteristics. The names of these groups and
285 their number fractions are shown in Table 1. The average mass spectral patterns of each

286 group are shown in Fig. S5.

287 Pure BC particles only presented strong signals for black carbon fragment ions (C_n^- and
288 C_n^+) in both positive and negative ion mass spectra without any signal of secondary
289 species like sulfate or nitrate, suggesting they were fresh BC particles that had not
290 undergone any aging process.

291 Biomass burning BC-containing (BBC) particles were characterized by an intense K^+
292 signal for +39 (the charge and m/z of the observed ion), +113 (K_2Cl^+) and +213 ($K_3SO_4^+$)
293 in the positive ion mass spectra and a strong signal for -26 (CN^-) and -42 (CNO^-) in the
294 negative ion mass spectra. A significant fragment of levoglucosan, -71 ($C_3H_3O_2^-$), was
295 also observed. Typical black carbon fragments (C_n^-) appeared in the negative ion mass
296 spectra. A high signal at -46 (NO_2), -62 (NO_3^-) and a relatively low signal at -97 (HSO_4^-)
297 were also observed, suggesting a significant accumulation of nitrate ions on BC particles
298 throughout the air pollution period. Potassium-containing soot is a well-established tracer
299 for biomass combustion (Andreae, 1983; Soto-Garcia et al., 2011). Water-soluble K^+ in
300 ambient particles measured by an online MARGA method correlated reasonably well
301 with the BBC particles number ($R^2=0.64$). Particles with similar mass spectral patterns
302 were previously observed in several urban field studies and assigned to biomass burning
303 sources (Moffet et al., 2008; Healy et al., 2012b; Bi et al., 2011).

304 BC internally-mixed with organic carbon and ammonium sulfate (BCOC-SOx) particles
305 exhibited signals for ammonium +17 (NH_3^+), +18 (NH_4^+), organic carbon +37 (C_3H^+),
306 +43 (CH_3CO^+), +50 ($C_4H_2^+$), +51 ($C_4H_3^+$), +61 ($CH_3C(OH)=OH^+$), +62 (($CH_3)_2NHOH^+$),
307 and a small signal for sodium +23 (Na^+) in the positive ion mass spectra, along with black
308 carbon fragment ions (C_n^+). There was a high signal for sulfate -97 (HSO_4^-) and a
309 relatively low signal for nitrate -46 (NO_3^-), -62 (NO_3^-) in the negative ion spectra. BC
310 internally-mixed with organic carbon and ammonium nitrate (BCOC-NOx) particles are
311 characterized by very similar positive ion mass spectra to BCOC-SOx, but exhibit lower
312 signals for sulfate and higher signals for nitrate in the negative ion spectra, i.e., -46
313 (NO_3^-), -62 (NO_3^-). BC particles with various intensities for organic carbon, nitrate and
314 sulfate were commonly detected in urban ATOFMS field studies (Moffet et al.,

315 2008;Ault et al., 2009;Dall’Osto and Harrison, 2006) and were assigned to traffic
316 emissions (Healy et al., 2012b).

317 K-rich BC-containing (KBC) particles exhibited strong signals for black carbon fraction
318 in both positive and negative ion mass spectra. This class also had signals for potassium
319 +39 (K^+), sodium +23 (Na^+) and ammonium +17 (NH_3^+), +18 (NH_4^+) in positive ion mass
320 spectra and nitrate -46 (NO_2^-), -62 (NO_3^-), sulfate -97 (HSO_4^-) in the negative ion mass
321 spectra. This class was detected from diesel vehicle emissions in a previous study by (Li
322 et al., 2013). The KBC exhibited pronounced diurnal variation, with two major peaks
323 during early morning (4:00- 7:00 LT) and night hours (20:00- 22:00 LT) (Fig. S7).
324 Shanghai municipal government regulates that the heavily loaded diesel trucks cannot go
325 into downtown area from 7:00- 20:00 LT. The diurnal variation of KBC is consistent
326 with the traffic flow of diesel trucks based on our results.

327 NOx can be used as a tracer of local traffic emissions in urban areas. In this study, the
328 NOx concentrations agreed well with the sum of KBC, BCOC-NOx and BCOC-SOx
329 particles numbers ($R^2=0.65$) (Fig. S8). Based on the above analysis, we believed that the
330 BBC came from biomass burning, KBC, BCOC-NOx and BCOC-SOx came from
331 traffic emissions.

332 We should note that SPAMS preferentially detected internally-mixed BC particles, and
333 had reduced detection efficiency for pure BC particles. The particles detected and
334 chemically analyzed by SPAMS range from 200 to 2000 nm in size, and the detection
335 efficiency decreases rapidly below 400 nm and above 1200 nm (Li et al., 2011). The
336 majority of the pure BC particles diameter are smaller than 200 nm in diameter (Kondo et
337 al., 2006), and therefore, they are missed by SPAMS.

338 **3.4 Mixing state and size distribution of internally-mixed BC particles**

339 **3.4.1 Temporal variations of internally-mixed BC particles**

340 A comparison of the internally-mixed BC particles number concentration between SP2
341 and SPAMS is given in Fig. 3. The agreement observed is reasonably good ($R^2 = 0.87$,

342 slope = 0.65) considering the combined experimental uncertainties of the methods.
343 Detected by SP2, the internally-mixed rBC particles accounted for approximately 70%
344 number fraction of BC-containing particles during the whole period. Moteki et al. (2007)
345 also found the internally-mixed rBC particles accounted for 63% number fraction of
346 BC-containing particles in the aged urban plume. The high correlation coefficient
347 indicates that we can use the two complementary techniques to analyze the mixing state
348 and chemical composition of internally-mixed BC particles with single particle resolution
349 at the same time (although not for the same particle since both methods are destructive).

350 The temporal variation of number size distribution and particle types changed rapidly and
351 intricately, as shown in Fig. 4. From 12:00 LT on 5 December to 00:00 LT on 7
352 December, the PM_{2.5} and rBC mass increased slowly to an extremely polluted state. The
353 number fraction of BBC particles also increased during this period (Fig. 4(b)) and the
354 D_p of rBC showed two distinct modes (Fig. 4(a)). Then, the BC-containing particles
355 number increased rapidly at 02:00 LT on 7 December. Presumably, boundary layer
356 compression during the night led the fast change of BC-containing particles. After that,
357 the number concentration of BC-containing particles exhibited diurnal variation, with two
358 major peaks at the rush hours, i.e., from 8:00-12:00 LT or from 16:00-20:00 LT.

359 **3.4.2 Size distribution and source apportionments of internally-mixed BC 360 particles**

361 Fig. 5(a) shows the entire diameter (D_p) number size distribution histogram of
362 internally-mixed rBC particles detected by SP2 during the entire sampling period. The
363 BC-containing particles were detected in both the condensation and droplet modes in this
364 study. The condensation mode peak was centered around ~230 nm and droplet mode
365 peak was centered around ~380 nm, with a boundary D_p around ~320 nm. The presence
366 of condensation mode (D_{va}= ~200-500 nm) and droplet mode (D_{va}= ~550-1200 nm) was
367 confirmed by the SPAMS data (Fig. 5(b)). Here the SPAMS size distribution was based
368 on the number fraction of BC-containing particles in all detected particles. Similar
369 particle size distributions were also found in other studies in China (Huang and Yu,
370 2008;Zhang et al., 2014).

371 The specific composition in condensation and droplet modes were quite different (Fig.5
372 (b)). BBBC particles exhibited a higher number fraction in the droplet mode than in the
373 condensation mode. Ammonium nitrate can condense on particle surfaces during
374 atmospheric transport if sulfate is fully neutralized and excess ammonia is available
375 (Riemer et al., 2004). The sulfate condensation on BC surfaces occurs soon after the BC
376 emission , while ammonium nitrate condensation occurs over longer timescales during
377 transport (Healy et al., 2012a). In this work, most KBC and BBBC particles and all the
378 BCOC-NOx particles showed stronger NO_3^- signals than SO_4^- signals (as shown in Fig.
379 S5), suggesting that most BC-containing were deeply aged. Based on the particle
380 classification and source apportionment analysis, the internally-mixed BC particles from
381 traffic emissions accounted for almost all of the particles observed in the condensation
382 mode. However, the particle sources in the droplet mode were more diverse, including
383 traffic emissions and biomass burning.

384 Previous studies revealed that different sources emit different core diameters for
385 rBC-containing particles (Liu et al., 2014;Takahama et al., 2014;Reddington et al.,
386 2013;Schwarz et al., 2008) and the aging processes affect the coating thickness (Laborde
387 et al., 2013;Liu et al., 2014). We identified the sources and estimated aging process of
388 rBC-containing particles by using 2-D image plot “fingerprint” of D_c and absolute
389 coating thickness (ACT) information. Fig. 5(c) shows the dependence of ACT on D_c ,
390 weighed by the number concentration. In the condensation mode, the particles were
391 characterized by small D_c values (~60-80 nm) with thin ACT (~50-130 nm). In
392 combination with the SPAMS information, these particles with small D_c and thin ACT
393 should be mainly from the traffic sources (Fig. 5(b)).

394 However, the droplet mode was very different from the condensation mode and showed a
395 diversity of sources. In the droplet mode, the “fingerprint” showed two peaks. The first
396 peak had small D_c values (~60-80 nm) and thick ACT (~130-300 nm). We assume that
397 the rBC-containing particles in the first peak were from traffic emissions. In previous
398 studies, the particles associated with traffic emissions had small core sizes and thin
399 coating thickness (Laborde et al., 2013;Liu et al., 2014). However, in this study, we

400 found that the rBC-containing particles from traffic could be highly-aged, resulting in a
401 much thicker coating than previously observed. This could be because polluted air
402 masses promote faster rBC aging processes (Matsui et al., 2013). The second peak
403 showed larger D_c (~80-130 nm) and thick ACT (~110-300 nm). These particles were
404 presumably from biomass burning. It has been reported using SP2 measurements that
405 fresh biomass burning rBC particles are thickly coated (Schwarz et al., 2008; Sahu et al.,
406 2012; Liu et al., 2014).

407 Since there was no clear-cut separation between traffic emissions and biomass burning
408 rBC-containing particle in droplet mode, it was hard to distinguish them when we just
409 used the core and shell information from SP2 (Liu et al., 2014). We selected those larger
410 core (80-130 nm) with thicker coating (120-300 nm) particles as biomass burning
411 particles and compared with the biomass burning particles number concentration from
412 SPAMS, as shown in Fig. S9. The good correlation ($R^2 = 0.71$) verified the conclusion
413 that the rBC-containing particles with bigger core and thicker coating were from biomass
414 burning. Even though these larger rBC-containing particles only accounted for less than
415 20% number fraction, they are likely to be more hygroscopic (Liu et al., 2013; Wang et al.,
416 2014) and be scavenged by wet deposition (Moteki et al., 2012). Besides, those particles
417 will also have greater potential to enhance the semi-direct effect (Koch and Del Genio,
418 2010) through interaction with cloud processes.

419 The diversity of sources of the droplet mode BC-containing particles was also detected in
420 SPAMS, as we discussed before. SPAMS data showed that, in the droplet mode, the
421 internally-mixed BC particles from traffic emissions were more abundant than those from
422 biomass burning (Fig. 5(b)). However, the SP2 data showed that particles with a small
423 core and thick ACT (major traffic emission) were less abundant than particles with a larger
424 core with thick ACT (major biomass burning) (Fig. 5(c)). As we discussed in part
425 2.1.2, rBC-containing particle with smaller cores are not efficiently detected by SP2,
426 which may result in an underestimation of the fraction of traffic emission rBC-containing
427 particles in the droplet mode.

428 The aging of traffic-emitted rBC-containing particles during the heavy air pollution
429 episode (12:00 LT, 5 December 2013 – 12:00 LT, 7 December 2013) was elucidated
430 using the temporal variation of relative coating thickness (RCT, entire particle
431 diameter/rBC core diameter, D_p/D_c) of rBC-containing particles ($D_c = 60\text{-}80 \text{ nm}$), as
432 shown in Fig. 6a. Note that we could only obtain optical sizing information from
433 sufficiently coated particles because of the SP2 obtained minimal detectable optical
434 diameter of $\sim 170 \text{ nm}$. From 16:00 LT to 22:00 LT on 5 December, the RCT of
435 rBC-containing particles and $\text{PM}_{2.5}$ concentration grew rapidly. Even though the SP2's
436 inlet was blocked from 23:00 LT on 5 December to 10:00 LT on 6 December due to the
437 extremely high PM mass loading, the data collected around that time suggest the
438 rBC-containing particles growth was continuous until 13:00 LT on 6 December. The
439 absolute coating growth rate was around 20 nm/hour during this period (16:00 LT, 5
440 December – 13:00 LT, 6 December).

441 Variations of the major chemical species in the vehicle-emitted BC-containing particles
442 (selected by SPAMS) were also analyzed. The relative peak areas of nitrate -63 (NO_3^-)
443 and organic carbon (i.e., +27 (C_2H_3^+), +43 (CH_3CO^+)) showed a relatively high level
444 during 16:00 LT on 5 December- 13:00 LT on 6 December (Fig. 6(b)). Guo et al. (2014)
445 observed that gaseous emissions of volatile organic compounds, nitrogen oxides from
446 urban transportation and sulfur dioxide from region industry were responsible for large
447 secondary particle matter formation in Beijing. Fig. S10 shows the mass concentrations
448 of SO_2 , NO_2 , the mass ratio of NO_2/SO_2 , MARGA-measured mass concentrations of
449 particulate sulfate and nitrate, and the mass ratio of $\text{NO}_3^-/\text{SO}_4^{2-}$ in PM_1 during the whole
450 sampling period. The average mass ratios of NO_2/SO_2 in gas phase and $\text{NO}_3^-/\text{SO}_4^{2-}$ in
451 particles phase were 2.8 and 1.4 respectively. During the heavy air pollution episode
452 (12:00 LT, 5 December 2013 – 13:00 LT, 6 December 2013), both NO_2 and particulate
453 nitrate increased dramatically along with the traffic emitted BC particle growth (as shown
454 Fig. 6), while SO_2 and sulfate remained at a relatively low level. Apparently, the gas to
455 particle conversion of NO_2 to nitrate played a more important role in the particle growth
456 during this pollution episode. In the previous field studies (Huebert et al., 1988; Yao et al.,
457 2002), the high mass ratio of $\text{NO}_3^-/\text{SO}_4^{2-}$ (>1.0) was regarded as a sign of dominant traffic

458 emission. Wang et al. (2015) found that the high mass ratio of NO₂/SO₂ resulting from
459 traffic emissions was a major reason in triggering the heavy haze in Shanghai. In this
460 work, the evaluation of BC-containing particles also suggested that high concentrations
461 of NO₂ and possibly volatile organics and their transformations play a vital role for
462 particle growth and the increase of PM loading in urban area especially during a heavy
463 pollution episode. Reductions in the emissions of gaseous precursors are critical for
464 remediation of the severe urban haze pollution in China.

465 **4 Conclusions**

466 In this study, we characterized BC-containing particles during a heavy air pollution
467 episode in Shanghai. The rBC mass loading in Shanghai was similar to other cities in
468 China but much higher than in other mega-cities around the world, with an average of 3.2
469 $\mu\text{g m}^{-3}$ and the peak value of 12.1 $\mu\text{g m}^{-3}$ at 04:26 LT on 7 December 2013. The rBC
470 mass accounted for 1.45% of PM_{2.5} mass on average. The number- and mass-weighted
471 BC core size distributions were around ~60-400 and 70-500 nm, with peaks around ~60
472 and ~200 nm, respectively.

473 Through SPAMS, we classified the BC-containing particles into 6 groups, according to
474 their mass spectral patterns. The pure BC particles accounted for 0.62% number fraction
475 of BC-containing particles (although this number could be underestimated because of the
476 low detection efficiency for pure BC in SPAMS). The BBBC particles from biomass
477 burning accounted for 25.57%. The KBC, BCOC-NOx and BCOC-SOx from traffic
478 emissions accounted for 70.18%. The remaining unidentified particles accounted for
479 3.63%.

480 The size distribution of internally-mixed rBC particles was bimodal. The condensation
481 mode mainly consisted of traffic emissions, which had a small core (~60-80 nm) with
482 thin ACT (~50-130 nm). The droplet mode included biomass burning and deeply aged
483 traffic-emitted rBC-containing particles. The biomass burning particles had larger core
484 sizes (~80-130 nm) with thick ACT (~110-300 nm) and the highly aged traffic emissions
485 had small core sizes (~60-80 nm) with thick ACT (~130-300 nm). It is rare to see the

486 traffic-emitted rBC growing so quickly to the droplet mode. The high concentration of
487 NO₂ and its rapid conversion to particulate nitrate accelerated the growth of
488 BC-containing particles and contributed to the high particle mass concentration during
489 this heavy air pollution episode.

490 The quantitative number and mass information provided by SP2 supplemented the
491 SPAMS chemical analysis in the entire experiment. The two complementary techniques
492 can detect the physical and chemical properties of BC aerosol with single particle
493 resolution. The combined use of SP2 and SPAMS would have potential of wider
494 applications for future projects.

495 **Acknowledgments**

496 This work was supported by the National Natural Science Foundation of China (91544224,
497 21177027), the Ministry of Science & Technology of China (2012YQ220113-4), the Science &
498 Technology Commission of Shanghai Municipality (14XD1400600), the Ministry of
499 Environmental Protection of China (201409008).

500

501

502 **References**

- 503
- 504 Adachi, K., Chung, S. H., and Buseck, P. R.: Shapes of soot aerosol particles and implications
505 for their effects on climate, *Journal of Geophysical Research: Atmospheres*, 115, D15206,
506 10.1029/2009JD012868, 2010.
- 507 Almeida, J., Schobesberger, S., Kurten, A., Ortega, I. K., Kupiainen-Maatta, O., Praplan, A. P.,
508 Adamov, A., Amorim, A., Bianchi, F., Breitenlechner, M., David, A., Dommen, J., Donahue, N.
509 M., Downard, A., Dunne, E., Duplissy, J., Ehrhart, S., Flagan, R. C., Franchin, A., Guida, R.,
510 Hakala, J., Hansel, A., Heinritzi, M., Henschel, H., Jokinen, T., Junninen, H., Kajos, M.,
511 Kangasluoma, J., Keskinen, H., Kupc, A., Kurten, T., Kvashin, A. N., Laaksonen, A., Lehtipalo,
512 K., Leiminger, M., Leppa, J., Loukonen, V., Makhmutov, V., Mathot, S., McGrath, M. J.,
513 Nieminen, T., Olenius, T., Onnela, A., Petaja, T., Riccobono, F., Riipinen, I., Rissanen, M.,
514 Rondo, L., Ruuskanen, T., Santos, F. D., Sarnela, N., Schallhart, S., Schnitzhofer, R., Seinfeld, J.
515 H., Simon, M., Sipila, M., Stozhkov, Y., Stratmann, F., Tome, A., Trostl, J., Tsagkogeorgas, G.,
516 Vaattovaara, P., Viisanen, Y., Virtanen, A., Vrtala, A., Wagner, P. E., Weingartner, E., Wex, H.,
517 Williamson, C., Wimmer, D., Ye, P. L., Yli-Juuti, T., Carslaw, K. S., Kulmala, M., Curtius, J.,
518 Baltensperger, U., Worsnop, D. R., Vehkamaki, H., and Kirkby, J.: Molecular understanding of
519 sulphuric acid-amine particle nucleation in the atmosphere, *Nature*, 502, 359-363,
520 10.1038/nature12663, 2013.
- 521 Andreae, M. O.: Soot Carbon and Excess Fine Potassium: Long-Range Transport of
522 Combustion-Derived Aerosols, *Science*, 220, 1148-1151, 10.1126/science.220.4602.1148,
523 1983.
- 524 Ault, A. P., Moore, M. J., Furutani, H., and Prather, K. A.: Impact of Emissions from the Los
525 Angeles Port Region on San Diego Air Quality during Regional Transport Events,
526 *Environmental Science & Technology*, 43, 3500-3506, 10.1021/es8018918, 2009.
- 527 Baumgardner, D., Kok, G., and Raga, G.: Warming of the Arctic lower stratosphere by light
528 absorbing particles, *Geophysical Research Letters*, 31, L06117, 10.1029/2003gl018883,
529 2004.
- 530 Baumgardner, D., Popovicheva, O., Allan, J., Bernardoni, V., Cao, J., Cavalli, F., Cozic, J.,
531 Diapouli, E., Eleftheriadis, K., Genberg, P. J., Gonzalez, C., Gysel, M., John, A., Kirchstetter, T.

- 532 W., Kuhlbusch, T. A. J., Laborde, M., Lack, D., Muller, T., Niessner, R., Petzold, A., Piazzalunga,
533 A., Putaud, J. P., Schwarz, J., Sheridan, P., Subramanian, R., Swietlicki, E., Valli, G., Vecchi, R.,
534 and Viana, M.: Soot reference materials for instrument calibration and intercomparisons: a
535 workshop summary with recommendations, *Atmos. Meas. Tech.*, 5, 1869-1887,
536 10.5194/amt-5-1869-2012, 2012.
- 537 Bi, X. H., Zhang, G. H., Li, L., Wang, X. M., Li, M., Sheng, G. Y., Fu, J. M., and Zhou, Z.: Mixing
538 state of biomass burning particles by single particle aerosol mass spectrometer in the
539 urban area of PRD, China, *Atmos. Environ.*, 45, 3447-3453,
540 10.1016/j.atmosenv.2011.03.034, 2011.
- 541 Bond, T. C., and Bergstrom, R. W.: Light absorption by carbonaceous particles: An
542 investigative review, *Aerosol Sci. Technol.*, 40, 27-67, 10.1080/02786820500421521,
543 2006.
- 544 Bond, T. C., Doherty, S. J., Fahey, D. W., Forster, P. M., Berntsen, T., DeAngelo, B. J., Flanner, M.
545 Ghan, S., Karcher, B., Koch, D., Kinne, S., Kondo, Y., Quinn, P. K., Sarofim, M. C., Schultz, M.
546 Schulz, M., Venkataraman, C., Zhang, H., Zhang, S., Bellouin, N., Guttikunda, S. K., Hopke, P.
547 K., Jacobson, M. Z., Kaiser, J. W., Klimont, Z., Lohmann, U., Schwarz, J. P., Shindell, D.,
548 Storelvmo, T., Warren, S. G., and Zender, C. S.: Bounding the role of black carbon in the
549 climate system: A scientific assessment, *Journal of Geophysical Research-Atmospheres*, 118,
550 5380-5552, 10.1002/jgrd.50171, 2013.
- 551 Cappa, C. D., Onasch, T. B., Massoli, P., Worsnop, D. R., Bates, T. S., Cross, E. S., Davidovits, P.,
552 Hakala, J., Hayden, K. L., Jobson, B. T., Kolesar, K. R., Lack, D. A., Lerner, B. M., Li, S. M., Mellon,
553 D., Nuaaman, I., Olfert, J. S., Petaja, T., Quinn, P. K., Song, C., Subramanian, R., Williams, E. J.,
554 and Zaveri, R. A.: Radiative Absorption Enhancements Due to the Mixing State of
555 Atmospheric Black Carbon, *Science*, 337, 1078-1081, 10.1126/science.1223447, 2012.
- 556 China, S., Mazzoleni, C., Gorkowski, K., Aiken, A. C., and Dubey, M. K.: Morphology and
557 mixing state of individual freshly emitted wildfire carbonaceous particles, *Nature
558 communications*, 4, 2122, doi:10.1038/ncomms3122, 2013.
- 559 Chung, S. H., and Seinfeld, J. H.: Global distribution and climate forcing of carbonaceous
560 aerosols, *Journal of Geophysical Research: Atmospheres*, 107, 4407,
561 10.1029/2001JD001397, 2002.

- 562 Corbin, J. C., Sierau, B., Gysel, M., Laborde, M., Keller, A., Kim, J., Petzold, A., Onasch, T. B.,
563 Lohmann, U., and Mensah, A. A.: Mass spectrometry of refractory black carbon particles
564 from six sources: carbon-cluster and oxygenated ions, *Atmos. Chem. Phys.*, 14, 2591-2603,
565 10.5194/acp-14-2591-2014, 2014.
- 566 Cross, E. S., Onasch, T. B., Ahern, A., Wrobel, W., Slowik, J. G., Olfert, J., Lack, D. A., Massoli, P.,
567 Cappa, C. D., Schwarz, J. P., Spackman, J. R., Fahey, D. W., Sedlacek, A., Trimborn, A., Jayne, J.
568 T., Freedman, A., Williams, L. R., Ng, N. L., Mazzoleni, C., Dubey, M., Brem, B., Kok, G.,
569 Subramanian, R., Freitag, S., Clarke, A., Thornhill, D., Marr, L. C., Kolb, C. E., Worsnop, D. R.,
570 and Davidovits, P.: Soot Particle Studies Instrument Inter-ComparisonProject Overview,
571 *Aerosol Sci. Technol.*, 44, 592-611, 10.1080/02786826.2010.482113, 2010.
- 572 Dall'Osto, M., and Harrison, R. M.: Chemical characterisation of single airborne particles in
573 Athens (Greece) by ATOFMS, *Atmos. Environ.*, 40, 7614-7631,
574 doi:10.1016/j.atmosenv.2006.06.053, 2006.
- 575 Du, H., Kong, L., Cheng, T., Chen, J., Du, J., Li, L., Xia, X., Leng, C., and Huang, G.: Insights into
576 summertime haze pollution events over Shanghai based on online water-soluble ionic
577 composition of aerosols, *Atmos. Environ.*, 45, 5131-5137,
578 <http://dx.doi.org/10.1016/j.atmosenv.2011.06.027>, 2011.
- 579 Feng, Y., Chen, Y., Guo, H., Zhi, G., Xiong, S., Li, J., Sheng, G., and Fu, J.: Characteristics of
580 organic and elemental carbon in PM2.5 samples in Shanghai, China, *Atmospheric Research*,
581 92, 434-442, <http://dx.doi.org/10.1016/j.atmosres.2009.01.003>, 2009.
- 582 Gao, R., Schwarz, J., Kelly, K., Fahey, D., Watts, L., Thompson, T., Spackman, J., Slowik, J.,
583 Cross, E., and Han, J.-H.: A novel method for estimating light-scattering properties of soot
584 aerosols using a modified single-particle soot photometer, *Aerosol Sci. Technol.*, 41,
585 125-135, 2007.
- 586 Guo, S., Hu, M., Zamora, M. L., Peng, J., Shang, D., Zheng, J., Du, Z., Wu, Z., Shao, M., Zeng, L.,
587 Molina, M. J., and Zhang, R.: Elucidating severe urban haze formation in China, *Proceedings
588 of the National Academy of Sciences*, 111, 17373-17378, 10.1073/pnas.1419604111, 2014.
- 589 Gysel, M., Laborde, M., Olfert, J. S., Subramanian, R., and Grohn, A. J.: Effective density of
590 Aquadag and fullerene soot black carbon reference materials used for SP2 calibration,
591 *Atmos. Meas. Tech.*, 4, 2851-2858, 10.5194/amt-4-2851-2011, 2011.

- 592 Healy, R. M., Chen, Y., Kourtchev, I., Kalberer, M., O'Shea, D., and Wenger, J. C.: Rapid
593 Formation of Secondary Organic Aerosol from the Photolysis of 1-Nitronaphthalene: Role
594 of Naphthoxy Radical Self-reaction, *Environmental Science & Technology*, 46, 11813-11820,
595 10.1021/es302841j, 2012a.
- 596 Healy, R. M., Sciare, J., Poulain, L., Kamili, K., Merkel, M., Muller, T., Wiedensohler, A.,
597 Eckhardt, S., Stohl, A., Sarda-Esteve, R., McGillicuddy, E., O'Connor, I. P., Sodeau, J. R., and
598 Wenger, J. C.: Sources and mixing state of size-resolved elemental carbon particles in a
599 European megacity: Paris, *Atmospheric Chemistry and Physics*, 12, 1681-1700,
600 10.5194/acp-12-1681-2012, 2012b.
- 601 Huang, X. F., and Yu, J. Z.: Size distributions of elemental carbon in the atmosphere of a
602 coastal urban area in South China: characteristics, evolution processes, and implications for
603 the mixing state, *Atmospheric Chemistry and Physics*, 8, 5843-5853, 2008.
- 604 Huang, X. F., Gao, R. S., Schwarz, J. P., He, L. Y., Fahey, D. W., Watts, L. A., McComiskey, A.,
605 Cooper, O. R., Sun, T. L., Zeng, L. W., Hu, M., and Zhang, Y. H.: Black carbon measurements in
606 the Pearl River Delta region of China, *Journal of Geophysical Research-Atmospheres*, 116,
607 10.1029/2010jd014933, 2011.
- 608 Huang, X. F., Sun, T. L., Zeng, L. W., Yu, G. H., and Luan, S. J.: Black carbon aerosol
609 characterization in a coastal city in South China using a single particle soot photometer,
610 *Atmos. Environ.*, 51, 21-28, 10.1016/j.atmosenv.2012.01.056, 2012.
- 611 Huebert, B., Mingxing, W., and Weixiu, L.: Atmospheric nitrate, sulfate, ammonium and
612 calcium concentrations in China, *Tellus B*, 40, 1988.
- 613 Jacobson, M. Z.: Strong radiative heating due to the mixing state of black carbon in
614 atmospheric aerosols, *Nature*, 409, 695-697,
615 http://www.nature.com/nature/journal/v409/n6821/supplinfo/409695a0_S1.html, 2001.
- 616 Jacobson, M. Z.: Effects of Externally-Through-Internally-Mixed Soot Inclusions within
617 Clouds and Precipitation on Global Climate†, *The Journal of Physical Chemistry A*, 110,
618 6860-6873, 10.1021/jp056391r, 2006.
- 619 John, W., Wall, S. M., Ondo, J. L., and Winklmayr, W.: MODES IN THE SIZE DISTRIBUTIONS
620 OF ATMOSPHERIC INORGANIC AEROSOL, *Atmospheric Environment Part a-General Topics*,
621 24, 2349-2359, 10.1016/0960-1686(90)90327-j, 1990.

- 622 Jongejan, P., Bai, Y., Veltkamp, A., Wye, G., and Slaninaa, J.: An Automated Field Instrument
623 for The Determination of Acidic Gases in Air, *Int. J. Environ. Anal. Chem.*, 66, 241-251, 1995.
624 Kanakidou, M., Seinfeld, J. H., Pandis, S. N., Barnes, I., Dentener, F. J., Facchini, M. C., Van
625 Dingenen, R., Ervens, B., Nenes, A., Nielsen, C. J., Swietlicki, E., Putaud, J. P., Balkanski, Y.,
626 Fuzzi, S., Horth, J., Moortgat, G. K., Winterhalter, R., Myhre, C. E. L., Tsagaridis, K., Vignati, E.,
627 Stephanou, E. G., and Wilson, J.: Organic aerosol and global climate modelling: a review,
628 *Atmos. Chem. Phys.*, 5, 1053-1123, 10.5194/acp-5-1053-2005, 2005.
629 Khalizov, A. F., Zhang, R., Zhang, D., Xue, H., Pagels, J., and McMurry, P. H.: Formation of
630 highly hygroscopic soot aerosols upon internal mixing with sulfuric acid vapor, *Journal of*
631 *Geophysical Research: Atmospheres*, 114, D05208, 10.1029/2008JD010595, 2009.
632 Koch, D., and Del Genio, A. D.: Black carbon semi-direct effects on cloud cover: review and
633 synthesis, *Atmospheric Chemistry and Physics*, 10, 7685-7696, 10.5194/acp-10-7685-2010,
634 2010.
635 Kondo, Y., Komazaki, Y., Miyazaki, Y., Moteki, N., Takegawa, N., Kodama, D., Deguchi, S.,
636 Nogami, M., Fukuda, M., Miyakawa, T., Morino, Y., Koike, M., Sakurai, H., and Ehara, K.:
637 Temporal variations of elemental carbon in Tokyo, *Journal of Geophysical Research: Atmospheres*,
638 111, D12205, 10.1029/2005JD006257, 2006.
639 Laborde, M., Schnaiter, M., Linke, C., Saathoff, H., Naumann, K. H., Mohler, O., Berlenz, S.,
640 Wagner, U., Taylor, J. W., Liu, D., Flynn, M., Allan, J. D., Coe, H., Heimerl, K., Dahlkotter, F.,
641 Weinzierl, B., Wollny, A. G., Zanatta, M., Cozic, J., Laj, P., Hitzenberger, R., Schwarz, J. P., and
642 Gysel, M.: Single Particle Soot Photometer intercomparison at the AIDA chamber, *Atmos.*
643 *Meas. Tech.*, 5, 3077-3097, 10.5194/amt-5-3077-2012, 2012.
644 Laborde, M., Crippa, M., Tritscher, T., Jurányi, Z., Decarlo, P. F., Temime-Roussel, B.,
645 Marchand, N., Eckhardt, S., Stohl, A., Baltensperger, U., Prévôt, A. S. H., Weingartner, E., and
646 Gysel, M.: Black carbon physical properties and mixing state in the European megacity
647 Paris, *Atmos. Chem. Phys.*, 13, 5831-5856, 10.5194/acp-13-5831-2013, 2013.
648 Lack, D. A., and Cappa, C. D.: Impact of brown and clear carbon on light absorption
649 enhancement, single scatter albedo and absorption wavelength dependence of black
650 carbon, *Atmospheric Chemistry and Physics*, 10, 4207-4220, 10.5194/acp-10-4207-2010,
651 2010.

- 652 Lan, Z. J., Huang, X. F., Yu, K. Y., Sun, T. L., Zeng, L. W., and Hu, M.: Light absorption of black
653 carbon aerosol and its enhancement by mixing state in an urban atmosphere in South
654 China, *Atmos. Environ.*, 69, 118-123, 10.1016/j.atmosenv.2012.12.009, 2013.
- 655 Lee, A. K. Y., Willis, M. D., Healy, R. M., Onasch, T. B., and Abbatt, J. P. D.: Mixing state of
656 carbonaceous aerosol in an urban environment: single particle characterization using the
657 soot particle aerosol mass spectrometer (SP-AMS), *Atmos. Chem. Phys.*, 15, 1823-1841,
658 10.5194/acp-15-1823-2015, 2015a.
- 659 Lee, A. K. Y., Willis, M. D., Healy, R. M., Wang, J. M., Jeong, C. H., Wenger, J. C., Evans, G. J., and
660 Abbatt, J. P. D.: Single particle characterization of biomass burning organic aerosol (BBOA):
661 evidence for non-uniform mixing of high molecular weight organics and potassium, *Atmos.*
662 *Chem. Phys. Discuss.*, 15, 32157-32183, 10.5194/acpd-15-32157-2015, 2015b.
- 663 Li, L., Huang, Z., Dong, J., Li, M., Gao, W., Nian, H., Fu, Z., Zhang, G., Bi, X., Cheng, P., and Zhou,
664 Z.: Real time bipolar time-of-flight mass spectrometer for analyzing single aerosol particles,
665 International Journal of Mass Spectrometry, 303, 118-124,
666 <http://dx.doi.org/10.1016/j.ijms.2011.01.017>, 2011.
- 667 Li, L., Tan, G. B., Zhang, L., Fu, Z., Nian, H. Q., Huang, Z. X., Zhou, Z., and Li, M.: Analysis of
668 Diesel Exhaust Particles Using Single Particle Aerosol Mass Spectrometry, *Chinese Journal*
669 *of Analytical Chemistry*, 41, 1831-1836, 10.3724/sp.j.1096.2013.30545, 2013.
- 670 Liu, D., Allan, J., Whitehead, J., Young, D., Flynn, M., Coe, H., McFiggans, G., Fleming, Z. L., and
671 Bandy, B.: Ambient black carbon particle hygroscopic properties controlled by mixing state
672 and composition, *Atmospheric Chemistry and Physics*, 13, 2015-2029,
673 10.5194/acp-13-2015-2013, 2013.
- 674 Liu, D., Allan, J. D., Young, D. E., Coe, H., Beddows, D., Fleming, Z. L., Flynn, M. J., Gallagher, M.
675 W., Harrison, R. M., Lee, J., Prevot, A. S. H., Taylor, J. W., Yin, J., Williams, P. I., and Zotter, P.:
676 Size distribution, mixing state and source apportionments of black carbon aerosols in
677 London during winter time, *Atmos. Chem. Phys. Discuss.*, 14, 16291-16349,
678 10.5194/acpd-14-16291-2014, 2014.
- 679 Matsui, H., Koike, M., Kondo, Y., Moteki, N., Fast, J. D., and Zaveri, R. A.: Development and
680 validation of a black carbon mixing state resolved three-dimensional model: Aging
681 processes and radiative impact, *Journal of Geophysical Research: Atmospheres*, 118,

- 682 2304-2326, 10.1029/2012JD018446, 2013.
- 683 McMeeking, G. R., Hamburger, T., Liu, D., Flynn, M., Morgan, W. T., Northway, M., Highwood,
684 E. J., Krejci, R., Allan, J. D., Minikin, A., and Coe, H.: Black carbon measurements in the
685 boundary layer over western and northern Europe, *Atmospheric Chemistry and Physics*, 10,
686 9393-9414, 10.5194/acp-10-9393-2010, 2010.
- 687 Moffet, R. C., de Foy, B., Molina, L. T., Molina, M. J., and Prather, K. A.: Measurement of
688 ambient aerosols in northern Mexico City by single particle mass spectrometry,
689 *Atmospheric Chemistry and Physics*, 8, 4499-4516, 2008.
- 690 Moffet, R. C., and Prather, K. A.: In-situ measurements of the mixing state and optical
691 properties of soot with implications for radiative forcing estimates, *Proceedings of the*
692 *National Academy of Sciences of the United States of America*, 106, 11872-11877,
693 10.1073/pnas.0900040106, 2009.
- 694 Moteki, N., Kondo, Y., Miyazaki, Y., Takegawa, N., Komazaki, Y., Kurata, G., Shirai, T., Blake, D.,
695 Miyakawa, T., and Koike, M.: Evolution of mixing state of black carbon particles: Aircraft
696 measurements over the western Pacific in March 2004, *Geophysical research letters*, 34,
697 2007.
- 698 Moteki, N., Kondo, Y., and Nakamura, S.: Method to measure refractive indices of small
699 nonspherical particles: Application to black carbon particles, *Journal of Aerosol Science*, 41,
700 513-521, 10.1016/j.jaerosci.2010.02.013, 2010.
- 701 Moteki, N., Kondo, Y., Oshima, N., Takegawa, N., Koike, M., Kita, K., Matsui, H., and Kajino, M.:
702 Size dependence of wet removal of black carbon aerosols during transport from the
703 boundary layer to the free troposphere, *Geophysical Research Letters*, 39, L13802,
704 10.1029/2012GL052034, 2012.
- 705 Moteki, N., Kondo, Y., and Adachi, K.: Identification by single - particle soot photometer of
706 black carbon particles attached to other particles: Laboratory experiments and ground
707 observations in Tokyo, *Journal of Geophysical Research: Atmospheres*, 2014.
- 708 Onasch, T. B., Trimborn, A., Fortner, E. C., Jayne, J. T., Kok, G. L., Williams, L. R., Davidovits, P.,
709 and Worsnop, D. R.: Soot Particle Aerosol Mass Spectrometer: Development, Validation, and
710 Initial Application, *Aerosol Sci. Technol.*, 46, 804-817, 10.1080/02786826.2012.663948,
711 2012.

- 712 Petzold, A., Ogren, J., Fiebig, M., Laj, P., Li, S.-M., Baltensperger, U., Holzer-Popp, T., Kinne, S.,
713 Pappalardo, G., and Sugimoto, N.: Recommendations for reporting "black carbon"
714 measurements, *Atmospheric Chemistry and Physics*, 13, 8365-8379, 2013.
- 715 Pöschl, U.: Atmospheric aerosols: Composition, transformation, climate and health effects,
716 *Angewandte Chemie International Edition*, 44, 7520-7540, 2005.
- 717 Ramanathan, V., and Carmichael, G.: Global and regional climate changes due to black
718 carbon, *Nature geoscience*, 1, 221-227, 2008.
- 719 Reddington, C. L., McMeeking, G., Mann, G. W., Coe, H., Frontoso, M. G., Liu, D., Flynn, M.,
720 Spracklen, D. V., and Carslaw, K. S.: The mass and number size distributions of black carbon
721 aerosol over Europe, *Atmospheric Chemistry and Physics*, 13, 4917-4939,
722 10.5194/acp-13-4917-2013, 2013.
- 723 Riemer, N., Vogel, H., and Vogel, B.: Soot aging time scales in polluted regions during day
724 and night, *Atmos. Chem. Phys.*, 4, 1885-1893, 10.5194/acp-4-1885-2004, 2004.
- 725 Sahu, L. K., Kondo, Y., Moteki, N., Takegawa, N., Zhao, Y., Cubison, M. J., Jimenez, J. L., Vay, S.,
726 Diskin, G. S., Wisthaler, A., Mikoviny, T., Huey, L. G., Weinheimer, A. J., and Knapp, D. J.:
727 Emission characteristics of black carbon in anthropogenic and biomass burning plumes
728 over California during ARCTAS-CARB 2008, *Journal of Geophysical Research-Atmospheres*,
729 117, 10.1029/2011jd017401, 2012.
- 730 Schnaiter, M., Linke, C., Mohler, O., Naumann, K. H., Saathoff, H., Wagner, R., Schurath, U.,
731 and Wehner, B.: Absorption amplification of black carbon internally mixed with secondary
732 organic aerosol, *Journal of Geophysical Research-Atmospheres*, 110,
733 10.1029/2005jd006046, 2005.
- 734 Schwarz, J. P., Gao, R. S., Fahey, D. W., Thomson, D. S., Watts, L. A., Wilson, J. C., Reeves, J. M.,
735 Darbeheshti, M., Baumgardner, D. G., Kok, G. L., Chung, S. H., Schulz, M., Hendricks, J., Lauer,
736 A., Karcher, B., Slowik, J. G., Rosenlof, K. H., Thompson, T. L., Langford, A. O., Loewenstein, M.,
737 and Aikin, K. C.: Single-particle measurements of midlatitude black carbon and
738 light-scattering aerosols from the boundary layer to the lower stratosphere, *Journal of*
739 *Geophysical Research-Atmospheres*, 111, 10.1029/2006jd007076, 2006.
- 740 Schwarz, J. P., Gao, R. S., Spackman, J. R., Watts, L. A., Thomson, D. S., Fahey, D. W., Ryerson,
741 T. B., Peischl, J., Holloway, J. S., Trainer, M., Frost, G. J., Baynard, T., Lack, D. A., de Gouw, J. A.,

- 742 Warneke, C., and Del Negro, L. A.: Measurement of the mixing state, mass, and optical size of
743 individual black carbon particles in urban and biomass burning emissions, *Geophysical*
744 *Research Letters*, 35, 10.1029/2008gl033968, 2008.
- 745 Schwarz, J. P., Spackman, J. R., Gao, R. S., Perring, A. E., Cross, E., Onasch, T. B., Ahern, A.,
746 Wrobel, W., Davidovits, P., Olfert, J., Dubey, M. K., Mazzoleni, C., and Fahey, D. W.: The
747 Detection Efficiency of the Single Particle Soot Photometer, *Aerosol Sci. Technol.*, 44,
748 612-628, 10.1080/02786826.2010.481298, 2010.
- 749 Seinfeld, J. H., and Pandis, S. N.: *Atmospheric chemistry and physics: from air pollution to*
750 *climate change*, John Wiley & Sons, 2012.
- 751 Shiraiwa, M., Kondo, Y., Iwamoto, T., and Kita, K.: Amplification of Light Absorption of Black
752 Carbon by Organic Coating, *Aerosol Sci. Technol.*, 44, 46-54, 10.1080/02786820903357686,
753 2010.
- 754 Song, X. H., Hopke, P. K., Fergenson, D. P., and Prather, K. A.: Classification of single particles
755 analyzed by ATOFMS using an artificial neural network, ART-2A, *Analytical Chemistry*, 71,
756 860-865, 10.1021/ac9809682, 1999.
- 757 Soto-Garcia, L. L., Andreae, M. O., Andreae, T. W., Artaxo, P., Maenhaut, W., Kirchstetter, T.,
758 Novakov, T., Chow, J. C., and Mayol-Bracero, O. L.: Evaluation of the carbon content of
759 aerosols from the burning of biomass in the Brazilian Amazon using thermal, optical and
760 thermal-optical analysis methods, *Atmospheric Chemistry and Physics*, 11, 4425-4444,
761 2011.
- 762 Stephens, M., Turner, N., and Sandberg, J.: Particle identification by laser-induced
763 incandescence in a solid-state laser cavity, *Appl. Optics*, 42, 3726-3736,
764 10.1364/ao.42.003726, 2003.
- 765 Takahama, S., Russell, L. M., Shores, C. A., Marr, L. C., Zheng, J., Levy, M., Zhang, R., Castillo, E.,
766 Rodriguez-Ventura, J. G., Quintana, P. J. E., Subramanian, R., Zavala, M., and Molina, L. T.:
767 Diesel vehicle and urban burning contributions to black carbon concentrations and size
768 distributions in Tijuana, Mexico, during the Cal-Mex 2010 campaign, *Atmos. Environ.*, 88,
769 341-352, 10.1016/j.atmosenv.2013.09.057, 2014.
- 770 Taylor, J. W., Allan, J. D., Liu, D., Flynn, M., Weber, R., Zhang, X., Lefer, B. L., Grossberg, N.,
771 Flynn, J., and Coe, H.: Assessment of the sensitivity of core/shell parameters derived using

772 the single-particle soot photometer to density and refractive index, *Atmos. Meas. Tech.*
773 *Discuss.*, 7, 5491-5532, 10.5194/amtd-7-5491-2014, 2014.

774 Wang, Q., Zhuang, G., Huang, K., Liu, T., Deng, C., Xu, J., Lin, Y., Guo, Z., Chen, Y., Fu, Q., Fu, J. S.,
775 and Chen, J.: Probing the severe haze pollution in three typical regions of China:
776 Characteristics, sources and regional impacts, *Atmos. Environ.*, 120, 76-88,
777 <http://dx.doi.org/10.1016/j.atmosenv.2015.08.076>, 2015.

778 Wang, X., Ye, X., Chen, H., Chen, J., Yang, X., and Gross, D. S.: Online hygroscopicity and
779 chemical measurement of urban aerosol in Shanghai, China, *Atmos. Environ.*, 95, 318-326,
780 <http://dx.doi.org/10.1016/j.atmosenv.2014.06.051>, 2014.

781 Willis, M. D., Healy, R. M., Riemer, N., West, M., Wang, J. M., Jeong, C. H., Wenger, J. C., Evans,
782 G. J., Abbatt, J. P. D., and Lee, A. K. Y.: Quantification of black carbon mixing state from traffic:
783 implications for aerosol optical properties, *Atmos. Chem. Phys. Discuss.*, 15, 33555-33582,
784 10.5194/acpd-15-33555-2015, 2015.

785 Yao, X., Chan, C. K., Fang, M., Cadle, S., Chan, T., Mulawa, P., He, K., and Ye, B.: The
786 water-soluble ionic composition of PM2.5 in Shanghai and Beijing, China, *Atmos. Environ.*,
787 36, 4223-4234, [http://dx.doi.org/10.1016/S1352-2310\(02\)00342-4](http://dx.doi.org/10.1016/S1352-2310(02)00342-4), 2002.

788 Ye, B., Ji, X., Yang, H., Yao, X., Chan, C. K., Cadle, S. H., Chan, T., and Mulawa, P. A.:
789 Concentration and chemical composition of PM2.5 in Shanghai for a 1-year period, *Atmos.*
790 *Environ.*, 37, 499-510, [http://dx.doi.org/10.1016/S1352-2310\(02\)00918-4](http://dx.doi.org/10.1016/S1352-2310(02)00918-4), 2003.

791 Zhang, G., Bi, X., He, J., Chen, D., Chan, L. Y., Xie, G., Wang, X., Sheng, G., Fu, J., and Zhou, Z.:
792 Variation of secondary coatings associated with elemental carbon by single particle
793 analysis, *Atmos. Environ.*, 92, 162-170, <http://dx.doi.org/10.1016/j.atmosenv.2014.04.018>,
794 2014.

795 Zhang, R., Khalizov, A. F., Pagels, J., Zhang, D., Xue, H., and McMurry, P. H.: Variability in
796 morphology, hygroscopicity, and optical properties of soot aerosols during atmospheric
797 processing, *Proceedings of the National Academy of Sciences*, 105, 10291-10296,
798 10.1073/pnas.0804860105, 2008.

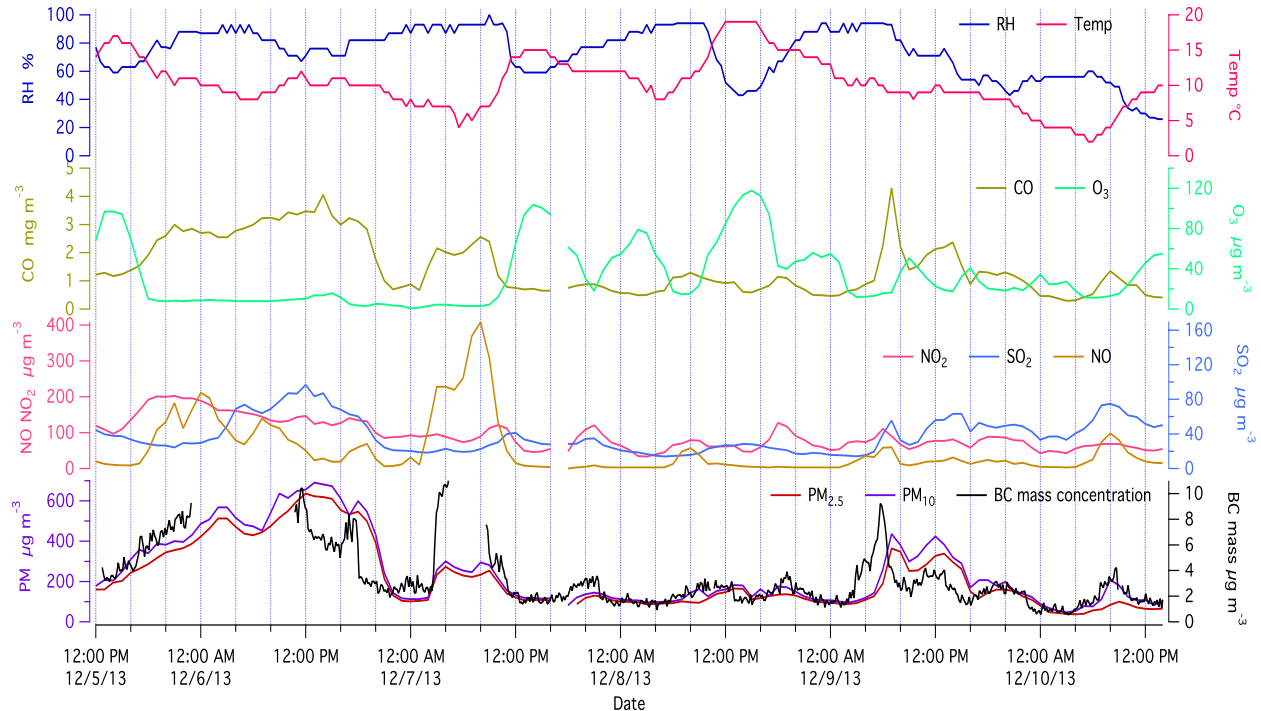
799

800 **Table 1.** Names, numbers and fractions of six types of BC-containing particles detected
801 by the SPAMS instrument.

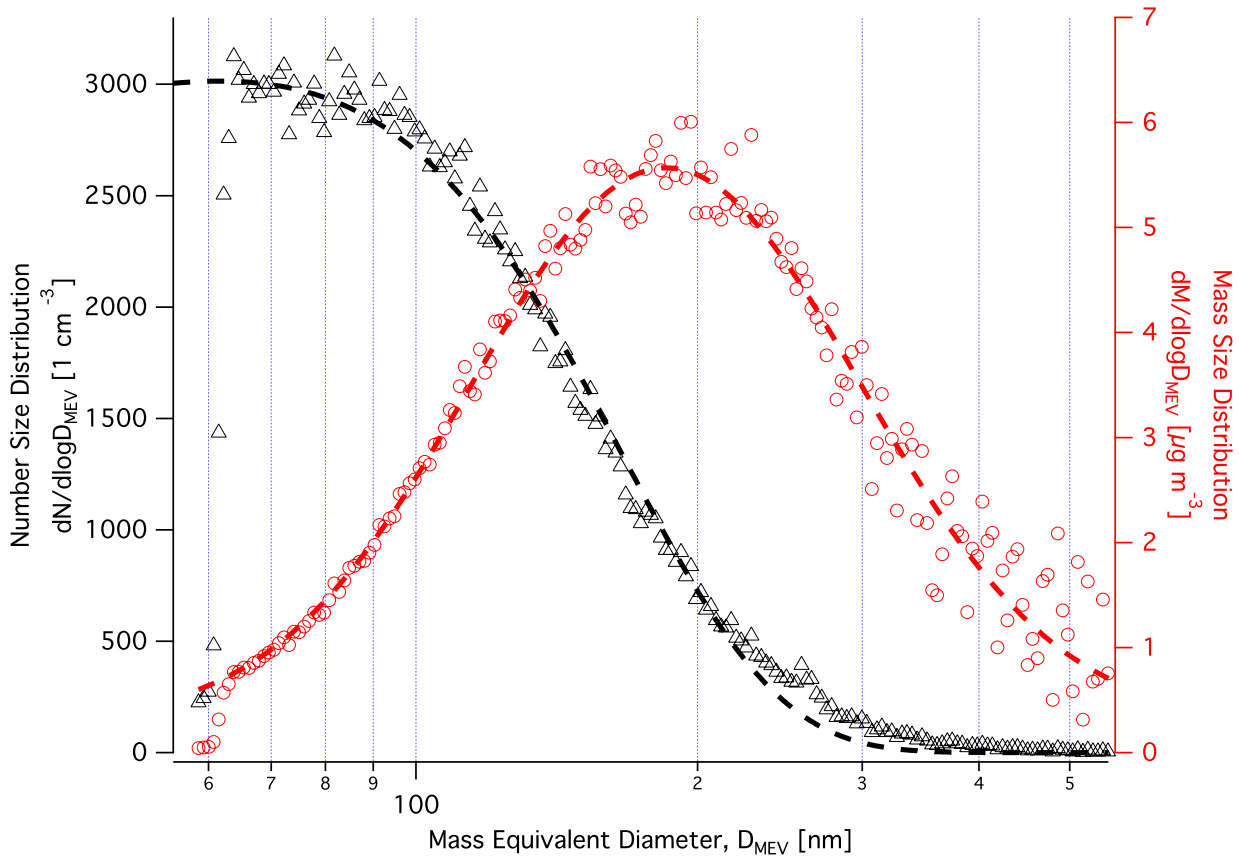
Group	Number of particles	Fraction of particles
Pure BC	535	0.62%
Biomass Burning BC-containing (BBC)	22 007	25.57%
K-rich BC-containing (KBC)	11 343	13.18%
BC internally-mixed with OC and ammonium nitrate (BCOC-NOx)	33 760	39.23%
BC internally-mixed with OC and ammonium sulfate (BCOC-SOx)	15 291	17.77%
Unidentified	3121	3.63%
Total BC-containing	86 057	100%

802

803

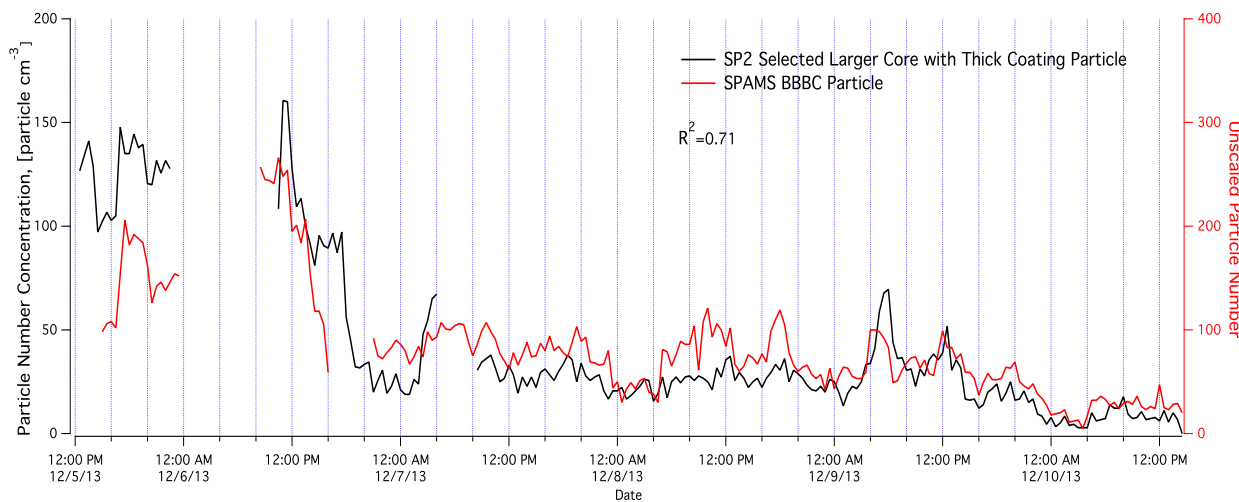


806 **Figure 1.** Temporal profiles of selected meteorological parameters (temperature,
 807 relative humidity) with 30 min resolution, gaseous pollutants (CO, O₃, SO₂, NO and NO₂),
 808 PM_{2.5} and PM₁₀ mass concentrations with 60 min resolution. The concentration of rBC
 809 mass (black trace in the bottom panel, 10 min resolution) was continuously measured by
 810 SP2.
 811



812

813 **Figure 2.** The measured rBC core mass size distribution and number size distribution are
 814 shown in open red and black markers, respectively. The log-normal fits to the observed
 815 distributions are shown by the dashed lines.

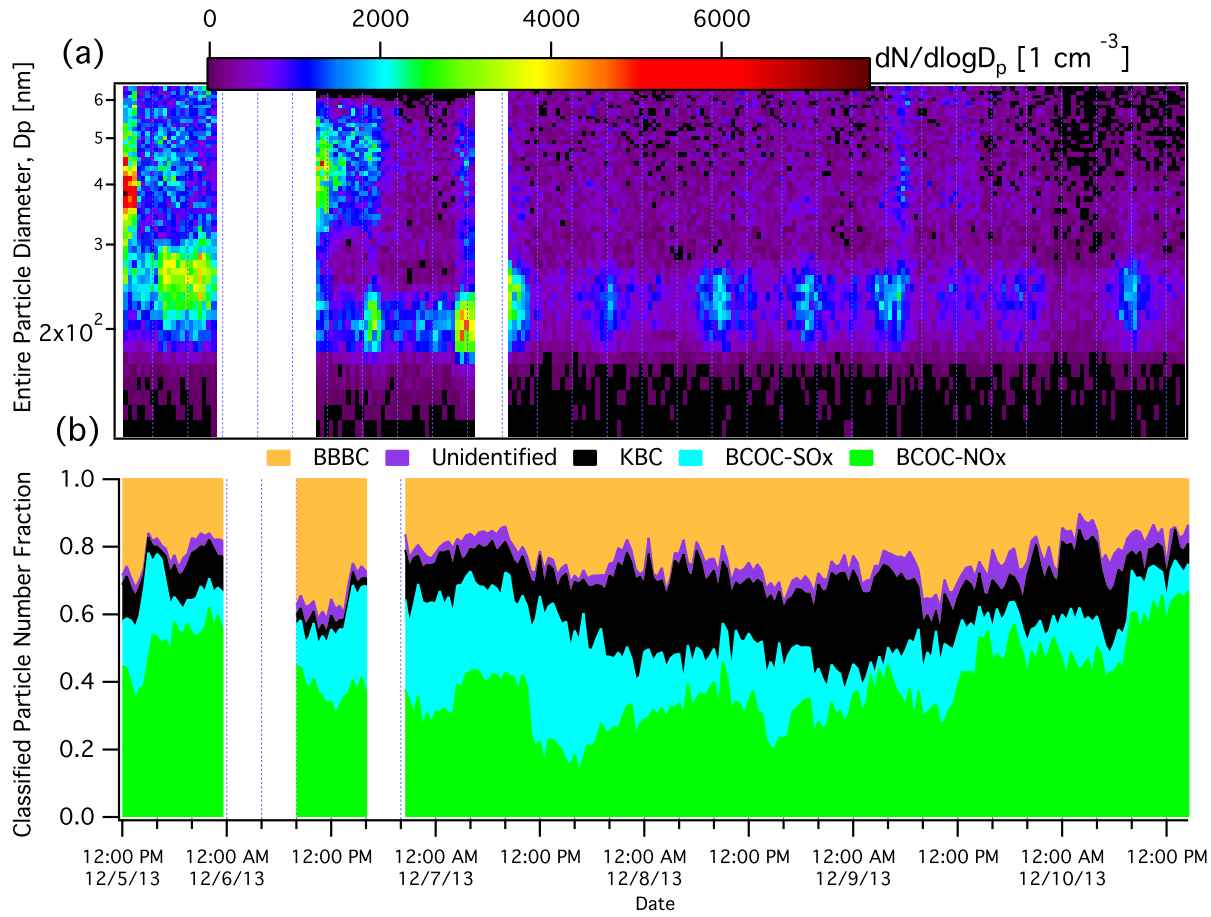


816

817 **Figure 3.** Comparison of the SPMAS-detected BC-containing particles and SP2-detected
 818 internally-mixed rBC-containing particles.

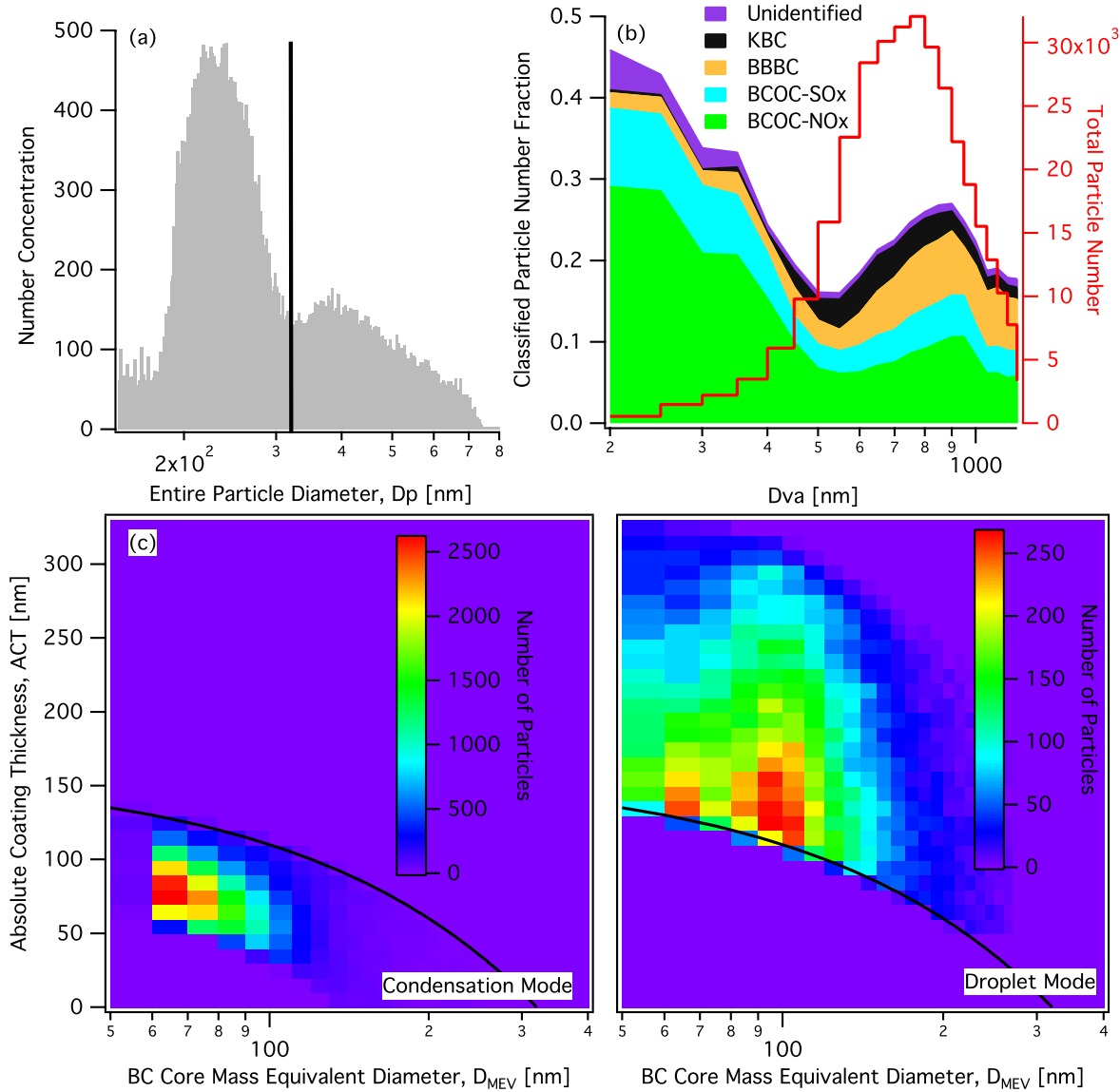
819

820



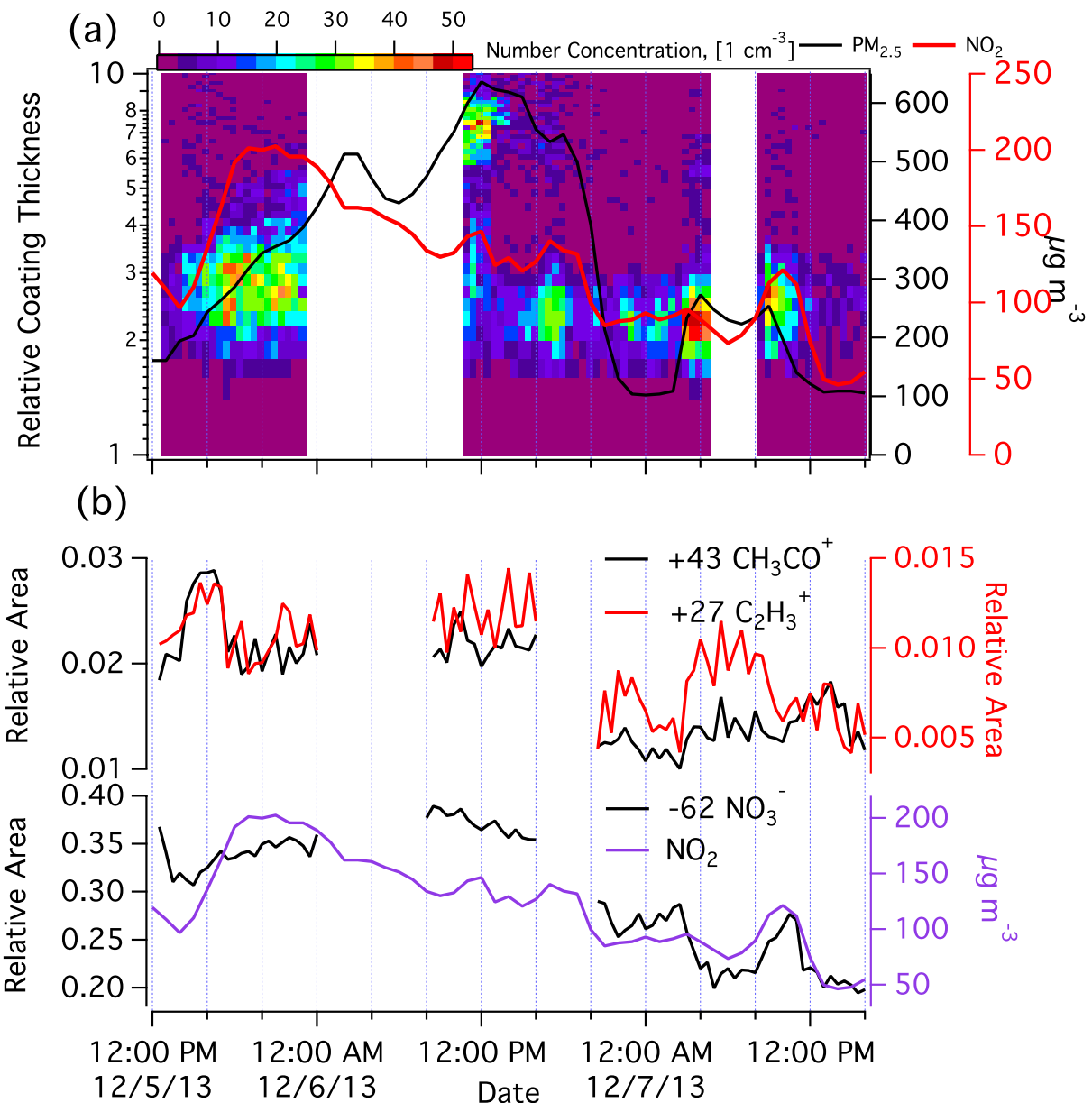
821

822 **Figure 4.** (a) Temporal variations of number and size distributions for rBC-containing
 823 particles detected by SP2 with 30 min resolution. (b) Temporal variation of number
 824 fractions of different BC-containing particle types with 10 min time resolution (detected
 825 by SPAMS).



826

827 **Figure 5.** (a) D_p number size distribution histogram for the SP2-detected rBC-containing
 828 particles. (b) D_{va} number fraction distribution of SPAMS-detected BC-containing
 829 particles color-coded by the particle type. (c) D_c and ACT with number size distribution
 830 in the condensation and droplet modes.



831

832 **Figure 6.** (a) Temporal variation of the relative coating thickness distribution of
 833 traffic-emitted rBC-containing particles (SP2) with resolutions of 0.2 RCT and 30 min
 834 and the temporal profile of NO₂ and PM_{2.5} concentrations with 60 min resolution. (b)
 835 Temporal variation of relative peak areas of +27 (C_2H_3^+), +43 (CH_3CO^+) and -62 (NO_3^-)
 836 of traffic-emitted BC-containing particles (SPAMS) and NO₂ concentration with 30 min
 837 resolution.